THE IMPORTANCE OF SPECIAL CORE ANALYSIS IN MODELLING REMAINING OIL SATURATION IN CARBONATE FIELDS

S.K. Masalmeh and X.D. Jing
Shell Technology Oman

ABSTRACT

An integrated study has been carried out to understand the field performance and remaining oil distribution of a number of heterogeneous and oil-wet carbonate reservoirs under waterflooding. Demonstrating the impact of basic rock characterization and special core analysis (SCAL) laboratory data on waterflood performance of a Cretaceous carbonate reservoir is the main focus of this paper.

The rock characterization programme includes measuring detailed permeability distribution along reservoir intervals and integration with geological facies modeling. The SCAL programme consists of drainage and imbition capillary pressure and relative permeability measurements for the predominant rock types using rock and fluid samples under representative reservoir conditions of pressure, temperature and wettability. To ensure data quality and repeatability, a combination of steady state with end-point bump floods and centrifuge techniques have been used for measuring the relative permeability curves extended to waterflood residual oil saturation. Numerical simulation was used to reconcile the various SCAL datasets and derive a consistent set of saturation functions.

The SCAL measurements took into consideration the importance of core sampling, cleaning and the proper procedures for obtaining reliable drainage capillary pressure data. We show that both imbition capillary pressure and relative permeability have major impact on the waterflood sweep efficiency and cross-flow between adjacent oil-wet layers and hence on the distribution of remaining oil saturation. An incorrect understanding of the distribution of remaining oil saturation may lead to ineffective well and reservoir management and IOR/EOR decisions.

INTRODUCTION

In the past few years, we have been working on understanding waterflooding performance in heterogeneous oil-wet carbonate reservoirs (Masalmeh et al., 2003 & 2007) with a focus on the impact of geological heterogeneity and imbition capillary curves. In this paper we will report on our ongoing study to include the impact of relative permeability curves on cross flow between reservoir layers and hence sweep efficiency and field-wide remaining oil saturation distribution.

In this study we combine conventional core analysis (porosity, permeability), mercury-air capillary pressure and special core analysis data (i.e., the imbibition Pc, relative permeability and residual oil saturation) with the aim to better predict water flooding performance. The capillary pressure data used in this paper are measured using mercury injection and centrifuge techniques. Mercury injection is frequently used for measuring drainage Pc curves as the technique is relatively cheap, fast and requires relatively straightforward data interpretation. The measured data, however, need to be converted to in situ reservoir conditions by taking into account the differences in interfacial tension and contact angle between the rock/fluid systems used in the laboratory and that found in reservoir. The multi-speed centrifuge method can be used for both drainage and imbibition Pc measurements using representative reservoir fluids. Compared with the porous-plate equilibrium technique, the centrifuge method is relatively fast, which is a clear advantage for studying carbonates with low matrix permeabilities. However, the design of the centrifuge experiment and the interpretation of the data are not straightforward and numerical simulation of centrifuge experiments is generally required to derive capillary pressure data (Maas and Schulte 1997). In this study we employed the steady state (with high-rate end point bumps), and centrifuge techniques to get the full relative permeability and imbibition capillary pressure curves using numerical simulation of SCAL experiments.

We will first present the experimental data and experimental procedures required to obtain representative capillary pressure and relative permeability curves. We then show the impact of such data on field simulations using 3-D sector models from a Cretaceous Middle East carbonate reservoir.

EXPERIMENTAL MEASUREMENTS

Drainage Capillary Pressure

Drainage capillary pressure is used for reservoir rock classification or rock typing and to initialise reservoir static model, i.e., to determine saturation as a function of height above free water level (FWL) in conjunction with saturation logs. Several authors have discussed the complexity of obtaining a consistent set of drainage capillary pressure curves from the different techniques available (Honarpour et al. 2004; Sallier and Hamon 2005; Masalmeh and Jing 2004 and 2006). Although the experimental procedures are well established, the measured drainage Pc curves using different techniques are not always consistent and conflicting data are often encountered (e.g., when comparing data from different fluid pairs for the same rock or data from different measurement techniques). One of the reasons for the discrepancies is due to the ineffective core cleaning (a particular challenge for carbonates) to establish correct wettability conditions mimicking the primary drainage process in the reservoir (Masalmeh and Jing, 2006 & 2007). Another uncertainty lies in the procedure to convert measured Pc curves using different fluid pairs and/or different experimental conditions. For example, the Hg-air Pc curves can be converted to oil-water drainage Pc curves using the following equation:

$$Pc_R = Pc_L \frac{\sigma_R \cos(\theta)_R}{\sigma_L \cos(\theta)_L} \qquad\qquad (1)$$

where σ is the interfacial tension (IFT) between the two fluids, θ is the contact angle, subscript L refers to laboratory (Hg-air) and R refers to reservoir (oil-water) fluids. For detailed review and discussion on relating mercury injection data to equivalent oil-water systems, see Morrow and Melrose (1991).

To ensure consistency of the measured data and take into account rock heterogeneity on the measured Pc curves, the mercury/air capillary pressure curves have been measured using core plugs of 15 mm in diameter and 22 mm long which have been drilled in the vicinity of the selected SCAL plugs used in the centrifuge experiments.

We reported previously (Masalmeh and Jing 2004, 2006) that the capillary pressures measured using centrifuge and mercury injection methods (after converting the data to water-oil equivalent Pc) showed a close match for samples that have been properly cleaned. For converting mercury-air Pc curves into water-oil or water-air Pc, both IFT and contact angle of different fluid pairs are substituted in equation (1). The IFTs between different fluids can be accurately measured using established techniques, however, contact angles cannot be measured directly on reservoir rocks. Contact angles measured on polished mineral surfaces are not likely to represent reservoir rocks even for the water-wet case due to the impact of surface roughness.

In the literature, contact angles of 140, 30, 0 and 0 have been used for mercury-air, reservoir oil-water, refined oil-water and water-air, respectively (Archer and Wall 1986, Honarpour et. al. 2004). We found no experimental or theoretical support evidence for these assumptions. In order to check the validity of these assumptions we have measured capillary pressure curves using four different fluid pairs, i.e., mercury-air, water-air, water-oil and water-decane on either the same samples or on adjacent small samples. We have also measured IFT between the different fluid pairs (used literature data for the mercury-air) at the different experimental conditions. Using equation (1), the only un-known is the ratio of the cosine of the contact angles. The measured IFT values between the different fluid pairs are 480, 72, 27 and 52 mN/m for mercury-air, water-air, water-oil and water-decane, respectively. The best match between the measured Pc curves was obtained using the same effective contact angle for the different fluid pairs in equation (1), i.e., $\cos(\theta)$ cancels out. Figure 1 shows a comparison between mercury-air and centrifuge water-oil, water-air and water-decane Pc curves on three different samples. The data presented here does not provide a contact angle value, however, it shows that the contact angle for each fluid pair can be considered to be the same. Note that contact angle in this study refers to an effective contact angle for the respective saturation direction (Dumore and Schols 1974).

These results confirm earlier findings (Masalmeh and Jing 2006, 2007) that: 1- for properly cleaned samples, capillary pressure curves measured using different fluid pairs can be converted using equation (1), 2- the difference between the water-oil capillary pressure and the mercury injection data can be used to check the efficiency of the cleaning method and 3- mercury-air Pc curves can be used to generate saturation height functions for both gas and oil reservoirs. However, it is always advisable to measure drainage capillary pressure using different techniques or fluid pairs to check whether the samples used for mercury injection is representative to the large SCAL sample used in water-oil measurements.

Imbibition Capillary Pressure
The impact of capillary forces on multiphase flow and hydrocarbon recovery has been studied extensively in the last few years [Masalmeh et. al. 2003, Masalmeh and Jing 2007 and references therein]. In this study, imbibition capillary pressure curves have been measured on more than 50 samples from the reservoir under study. The experimental procedure, data interpretation and a procedure to correlate drainage and imbibition capillary pressure curves and the impact of imbibition Pc on the sweep efficiency and remainig oil saturation distribution have been published elsewhere [Masalmeh and Jing, 2006, 2007]. In this work we show the combined impact of both imbibition capillary pressure and relative permeability on the waterflood sweep efficiency and cross-flow behaviour between adjacent oil-wet layers and hence on the distribution of remaining oil saturation.

Relative Permeability Curves
Relative permeability curves were measured using a combination of steady state (including high rate end-point bumps) and centrifuge techniques to derive the complete relative permeability curves to the residual oil saturation. Numerical simulation was used to both design the experiments and interpret the experimental raw data. The experiments were performed as follows:
   1- Clean and saturate the samples to 100% water.
   2- Use air-water porous plate to initialise the samples at connate water saturations of 6-10%. Using porous plate ensures homogeneous saturation profile in the samples at the beginning of the experiment.
   3- Displace air by oil and age the samples at reservoir pressure and temperature to restore reservoir wettability.
   4- Measure oil permeability at connate water at reservoir pressure and temperature.
   5- Use the following different water fractional flows (1%, 5%, 15%, 50%, 85%, 95%, 99%, 100%) with a total flow rate of 30 cc/hour for low permeability samples and 50 cc/hour for higher permeability samples (>100 mD).
   6- At the end of the steady state experiment, perform bump floods by increasing the flow rate to 200 cc/hour and 500 cc/hour, respectively. These high rates serve to reduce the remaining oil saturation, extends the water relative permeability curve to lower oil saturation and decrease capillary end effect. The high rates are selected such that the capillary number of 10^{-5} is not violated.

7- On a twin sample measure imbibition capillary pressure curve using multi-speed centrifuge technique. Use imbibition capillary pressure to perform numerical interpretation of the steady state raw data to get the water and oil relative permeability curves. The derived relative permeabilities were used in a further iteration of multi-speed centrifuge simulation ensure both experiments are history matched simultaneously using one set of relative permeability and capillary pressure curves.
8- Perform water-oil imbibition single speed centrifuge experiment (on the same sample used in the multi-speed experiment) to get the tail end of the oil relative permeability curve.
9- Measure both water permeability at residual oil saturation and oil permeability at connate water on all the samples used in the centrifuge experiment.

EXPERIMENTAL RESULTS AND DISCUSSION

Steady state experiments were performed on eight samples selected from the three main rock types identified in a previous publication (Masalmeh and Jing 2007). The characteristics of the samples are shown in Table 1. Figure 2(a-b) show the measured centrifuge data in multi-speed and single-speed modes, respectively, against the simulated production curves. The same set of imbibition capillary pressure and relative permeability curves matched all the multi-phase flow experiments including both steady-state and centrifuge performed on the same (or twin) sample.

For all the samples used in the centrifuge, both oil and water relative permeability end points were measured at the end of drainage and imbibition centrifuge experiments. As shown in Figure 3, the data set show the oil end point generally in the range of 0.8 to 1 (except a few cases where data scattering leads to krow>1 due to measurement accuracies) and the water end point in the range of 0.6 to 0.8. There is hardly any trend of end point oil and water relative permeabilities against either permeability or porosity of the samples. There is also no clear trend against pore size distributions or drainage capillary pressure curves. Therefore, no attempt was made to correlate relative permeability end points with porosity, permeability or rock type in the subsequent reservoir simulation study. The experimental measured average values were used with the associated uncertainty ranges.

The raw experimental data were quality checked at each fractional-flow step in the experiment. For example, the saturation profile of all the samples at connate water was checked and validated (using x-ray scanning) before starting the steady state experiment to ensure homogeneous saturation profiles. The saturation profile and pressure drop of the steady state experiment at each fractional flow were checked against stability criteria before moving to the next fractional flow step. Figure 4 shows an example of pressure drop and saturation profile as well as the obtained history match from one of the steady state experiments. As shown in the figure, both pressure equilibrium and homogeneous saturation profile was observed at the end of each fractional-flow step. As the water saturation increases, capillary end effect is observed which results in high oil saturation towards the end of the plug sample. As the flow rate increases (the two bump rates), the

capillary end effect decreases (due to the change of viscous/capillary force balance) but does not disappear. Numerical interpretation of raw data was performed using MoReS (Shell in-house simulator). The capillary pressure used for numerical interpretation was either measured on twin sample (as discussed above) or derived from drainage capillary pressure using the procedure published in Masalmeh and Jing (2007).

Figures 5-7 show the relative permeability curves measured on the eight samples, for rock types I, II and III, respectively. The relative permeability curves shown in Figures 5-7 do not strictly follow a Corey function. We found that the oil relative permeability curves could be fitted with a modified Corey function (Masalmeh et. al 2006) where the Corey exponent varied between 4 to 4.8 and the variable c_o is in the range of 0 to 0.0003. The water relative permeability curves show more spread and a best fit of the data was obtained using water Corey in the range of 2.0 to 4.2 for the different samples. More work is needed to understand the reasons behind such a spread.

As discussed in earlier publications (Masalmeh and Jing 2006 and 2007), all the samples from the reservoir under study showed no noticeable water spontaneous imbibition confirming the oil-wet character. An apparent advanced oil-water contact angle of 110-120 was calculated for imbibition from the measured imbibition and drainage capillary pressure curves. The high oil Corey exponent found for most of the samples is qualitatively expected based on such wetting conditions. However, the high water Corey exponent found for some of the samples is not expected, especially for rock types I and III. This shows that the relative permeability is not just dependent on wettability but also on pore size distributions and an oil-wet rock may still have a high water Corey exponent. Further research is in progress to understand and model the relative permeability behaviour of this oil-wet carbonate reservoir.

Figure 8 shows oil relative permeability curves constructed from the combination of steady state and centrifuge technique for two different samples. The data show that when including the bump rates and through numerical interpretation the steady state experiment covers most of the saturation range and is in very good agreement with the centrifuge data. However, the oil relative permeability obtained using analytical interpretation of the raw data from the steady state experiment covers up to water saturation of 60-70% maximum.

The above shows that proper design and interpretation of steady state experiment can cover most of the relative permeability curve. The centrifuge technique complements the oil relative permeability steady state data and when both multi-speed and single-speed experiments are performed on the same plug the oil relative permeability can be reasonably defined through centrifuge alone. However, the steady state is always required to define the water relative permeability curve which can not be obtained by the centrifuge.

FIELD CASE

The measured conventional and special core analysis data have been used in simulation models to study the impact of relative permeability and capillary pressure on (1) water flooding and water cross-flow between layers of heterogeneous carbonate reservoirs and (2) sensitivity of waterflooding and remaining oil saturation distribution to permeability heterogeneity.

A ¼ symmetry element of an inverted 5-spot sector model was constructed. The simulation work was performed using a 3D model of 48 layers (48×25×25) and 50 m in total thickness. The thickness of the individual layers of the model varies between ~0.3 to 3 m, and the grid size in the x and y directions is 20×20 m. A vertical injector was placed in one corner of the model and a vertical producer was placed in the diagonally opposite corner. Initial fluid distributions were assigned to the model using drainage capillary pressure curves and switched to imbibition capillary pressure when water flood started.

The reservoir can be represented as a layer-cake type reservoir where strata measuring a meter or below in thickness can be correlated field wide, often over tens of kilometres. The overall permeability increases towards the top of the reservoir. The reservoir consists of two main bodies, i.e. an upper zone (high permeable layers inter-bedded in between low permeable layers) and a lower zone of low permeability layers. In the rest of the paper these two zones will be referred to as the upper and lower zones. The average permeability of the upper zone is some 10-100 times higher than that of the lower zone. For more details on this field see Masalmeh et. al. (2003).

Figure 9 shows two different permeability profiles (perm 1 and perm 2) at the location of observation wells 1&2, where the first permeability model (perm 1) shows higher permeability contrast. The proper use of capillary pressure (both drainage and imbibition) on fluid distribution and sweep efficiency was discussed previously (Masalmeh et. al. 2003 and Masalmeh and Jing 2007) where it was demonstrated that for heterogeneous oil-wet or mixed-wet reservoirs: 1- Capillary pressure is very important and may act as a barrier, preventing cross flow between the different layers leading to poor sweep efficiency and 2- The waterflood performance and remaining oil saturation are also strongly dependent on the permeability contrast between the different layers. In this study we report on the combined impact of relative permeability and capillary pressure curves on water flooding performance.

The impact of different relative permeability curves on oil recovery and remaining oil saturation distribution is evaluated using two relative permeability models (RLP1 and RLP2) and two capillary pressure models (Pc1 and Pc2) as shown in Figure 10. The figure shows examples Pc curves of RRT2 and RRT3 to illustrate the contrast for the different rock types. The first relative permeability model (RLP1) is our best initial estimate using analogue database values before conducting the current SCAL program. It was generated based on analogue experience calibrated with relative permeability end point measurements and limited centrifuge data.

A Corey model was used with 3 and 4 taken for water and oil Corey exponent, respectively. The second relative permeability model (RLP2) is generated after incorporating the newly acquired SCAL data. An example of relative permeability curves for RRT2 and RRT3 are shown in Figure 11.

Figure 12 shows the recovery factor of the upper zone, lower zone, total recovery and the water cut for the four runs using permeability model 1 (RLP1&RLP2 with Pc1, RLP1&RLP2 with Pc2). The figure shows ~10 and ~20 saturation units difference in recovery factor from the lower zone for scenarios 1&2 (runs with Pc1 model) and scenarios 3&4 (runs with Pc2 model), respectively. Figure 13 shows the saturation distribution at the location of observation well 2 (located half way between the injector and the producer) after injecting 1 pore volume of water. The two figures show that relative permeability curves have more significant impact for the case of Pc2 model which has a less significant imbibition Pc contrasts between upper and lower layers. For the runs with the first Pc model (Pc1), capillary forces act as barrier and limits cross flow between upper and lower zones. Therefore the impact of relative permeability curves is limited. For the Pc model 2, more cross flow takes place (lower contrast between the capillary pressure curves for the different rock types) and relative permeability curves enhances the cross flow between the upper and the lower zones.

Figures 14-15 show the recovery factor and the saturation profiles, respectively, of two more runs using permeability model 2, Pc model 1 and relative permeability models 1&2. Even with a permeability contrast of more than a factor 20 between the lower and upper zone, the recovery from the lower zones is significantly higher than those shown in Figure 12 (Pc1_RLP1 and Pc1_RLP2 runs). The data in Figures 14-15 show that the impact of both Pc curves and relative permeability (within the range tested in this study) is negligible. The results shown here demonstrate the value of detailed mechanistic simulation modelling in optimally design fit for purpose SCAL programs for this type of reservoirs.

CONCLUSIONS

1. The primary drainage Pc curves measured using two different methods (mercury injection vs. centrifuge oil-brine) and different fluid pairs (mercury-air, water-air, water-decane and water-air) have been compared for the same plugs from different porosity and permeability ranges. Close agreement between the Pc curves has been observed if the core samples are thoroughly cleaned and measured IFT values and the same contact angle for the different fluid pairs are used.
2. A combination of steady state (with high-rate bump bloods) and centrifuge techniques have been used to measure both water and oil relative permeability curves. A close agreement was found between the oil relative permeability curves measured by steady state and the centrifuge technique, see Fig. 8.
3. Numerical simulation and history matching of experimental SCAL raw data is a vital tool to get proper relative permeability and capillary pressure curves.

However, history matching can only add value when quality experimental data is available as it cannot compensate for poor measurements.

4. For this reservoir, the oil relative permeability curves for the different samples from different rock types and permeability ranges selected have little variation. However, more spread is observed for the water relative permeability curves. More work is needed to understand the reasons behind such a spread.

5. The effect of relative permeability and capillary pressure curves is interlinked. For the cases of large contrast between the capillary pressure curves, the cross flow between the different layers is limited and relative permeability has less significant impact. However, for the case of lower contrast between the capillary pressure curves, the relative permeability has much more impact on fluid cross flow between the different layers.

6. This work demonstrates the value of SCAL data (in combination with detailed static and dynamic modelling) in assessing water flooding performance and remaining oil saturation distribution for a heterogeneous oil-wet carbonate reservoir. Proper modelling and prediction of waterflood baseline is a pre-requisite for any subsequent IOR/EOR options.

ACKNOWLEDGEMENTS

REFERENCES
Archer, J.S. and Wall, C.G.: *Petroleum Engineering Principles and Practice*, Graham & Trotman, (1986).

Dumore, J.M. and Schols, R.S.: "Drainage Capillary Pressure Functions and the Influence of Connate Water", SPEJ (1974) 437-444.

Honarpour, M.M., Djabbarah, N.F. and Kralik, J.G.: "Expert-Based Methodology for Primary Drainage Capillary Pressure Measurements and Modelling", SPE 88709 presented at the ADIPEC conference, Abu Dhabi, (2004).

Maas, J.G. and Schulte A.M.: "Computer Simulation of Special Core Analysis (SCAL) Flow Experiments Shared on the Internet", SCA-9719 presented at the SCA 1997 conference, Calgary, Canada (1997).

Masalmeh, S.K., Jing, X.D., van Vark, W., van der Weerd, H. Christiansen, S. and van Dorp, J.: "Impact of SCAL on Carbonate Reservoirs: How Capillary Forces Can Affect Field Performance Predictions" SCA 2003-36 presented at the SCA 2003 conference, Pau, France, October (2003).

Masalmeh, S.K., Jing, X.D.: "Carbonate SCAL: Characterization of Carbonate Rock Types for Determination of Saturation Functions and Residual Oil Saturation", SCA-08 presented at the SCA 2004 conference, Abu Dhabi, October (2004).

Masalmeh, S.K. and Jing, X.D. "Capillary Pressure Characteristics of Carbonate Reservoirs: Relationship between Drainage and Imbibition Curves", SCA 2006-16, Reviewed Proc. International Symposium of the Society of Core Analysts, Trondheim, Norway, 12-16 September, (2006).

Masalmeh, S.K., Abu Shiekah, I. and Jing, X.D.: "Improved Characterization and Modeling of Capillary Transition Zones in Carbonate Reservoirs", SPE paper 109094, SPE Reservoir Evaluation & Engineering, Vol. 10 (2): 191-204 APR (2007).

Masalmeh, S.K. and Jing, X.D.: "Improved Characterisation and Modelling of Carbonate Reservoirs for Predicting Waterflooding Performance", SPE paper 11722_PP, presented at the at the International Petroleum Technology Conference held in Dubai, U.A.E., 4–6 December (2007).

Morrow, N.R. and Melrose, J.C.: "Application of Capillary Pressure Measurements to the Determination of Connate Water Saturation", *Interfacial Phenomena in Petroleum Recovery*, N.R. Morrow (ed.), Marcel Dekker, New York City (1991) 257-287.

Sallier, B. and Hamon, G.: "Micritic Limestones of the Middle East: Influence of Wettability, Pore Network and Experimental Techniques on Drainage Capillary Pressure", SCA2005-08 presented at the SCA 2005 conference, Toronto, Canada, (2005).

Table 1: Samples characteristics

id	Por	Kair	Kw
	%	(mD)	(mD)
1	29.8	182	127
2	26.8	292	210
3	25.9	12.3	8.5
4	29.9	38.8	21.7
5	27.6	14.6	9.4
6	31.6	26.4	17.9
7	30.0	11.1	6.77
8	29.4	8.1	4.1
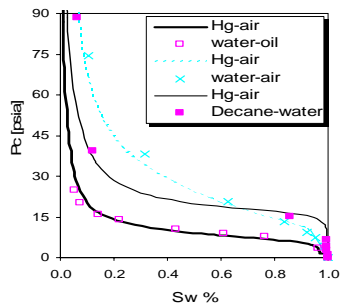
Figure 1: Comparing centrifuge oil-water, gas-water and decane-water Pc (symbols) to Hg-air Pc (lines). The measurements were done on different samples. Hg-air data is scaled with IFT to water-oil, water-air and decane-water, respectively.
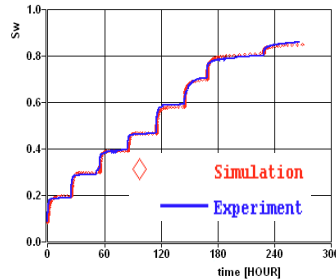
Figure 2a: History match of centrifuge multi-speed data.
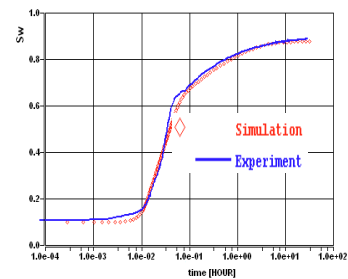
Figure 2b: History match of centrifuge single-speed data.
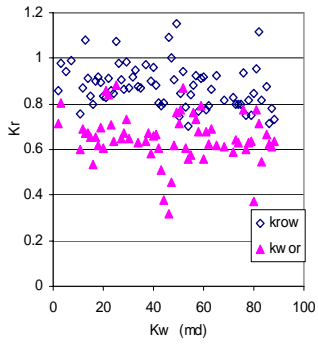
Figure 3: Water and oil permeability end points.
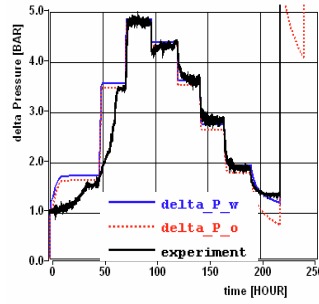
Figure 4a: History match of steady state data: pressure drop.
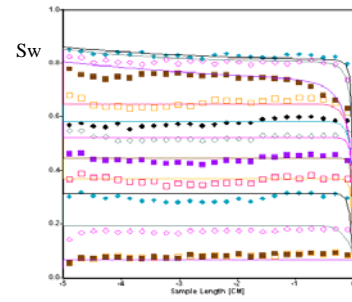
Figure 4b: History match of steady state data: saturation profile, experimental data in symboles and simulation in solid lines.
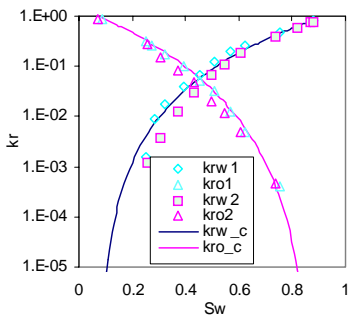
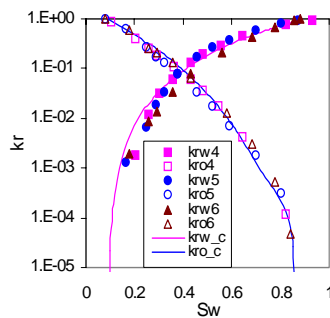Figure 5: Relative permeability curves of RRT1, solid line is a (modified) Corey fit.

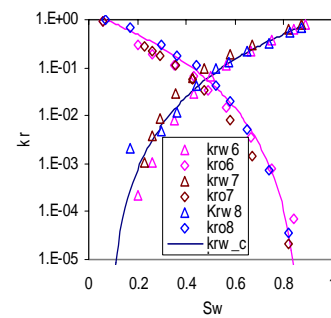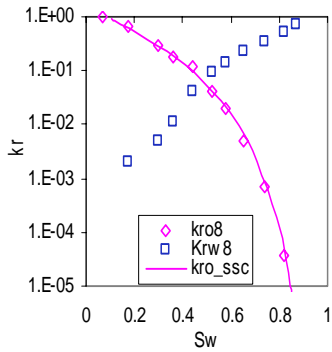Figure 6: Relative permeability curves of RRT2, solid line is a (modified) Corey fit.

Figure 7: Relative permeability curves of RRT3, solid line is a (modified) Corey fit.

Figure 8: Compare steady state (symbols) and centrifuge (solid line) relative permeability curve of sample 8.
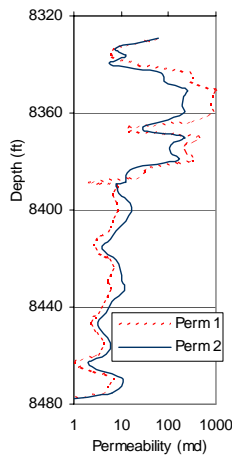
Figure 9a: Permeability profile at the location of observation well 1 located between injector and producer.
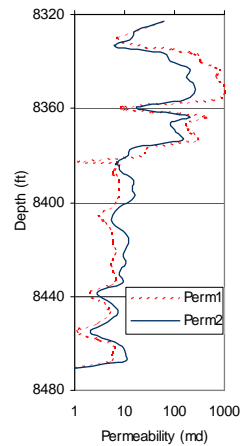
Figure 9b: Permeability profile at the location of observation well 2 located between injector and producer.
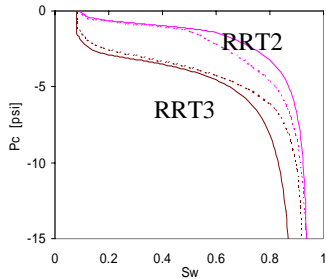
Figure 10: Capillary pressure models (Pc1 is solid line and Pc2 is dashed line) for RRT2 and RRT3.
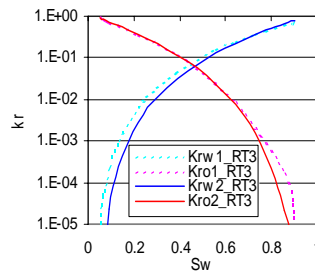
Figure 11: Relative permeability of RRT 3 from relative permeability models RLP1&RLP2.
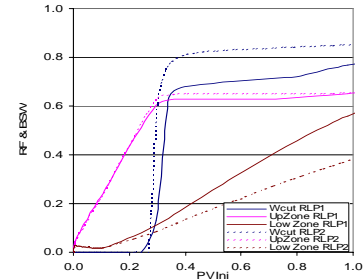
Figure 12a: Recovery factor of the upper and lower zones and water cut of two different runs using perm1, Pc1 and RLP1&RLP2.
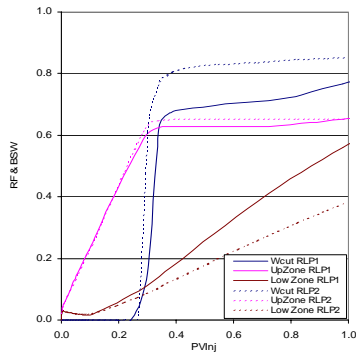
Figure 12b: Recovery factor of the upper and lower zones and water cut of two different runs using perm1, Pc2 and RLP1&RLP2.
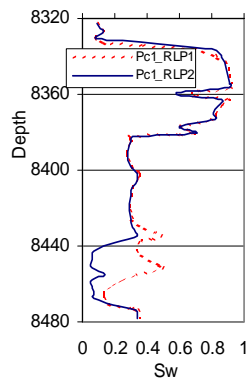
Figure 13a: Saturation profile after injecting 1 PV of water at the location of observation well 2 which is half way between injector and producer (perm 1 and Pc1).
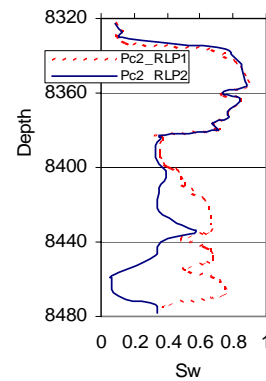
Figure 13b: Saturation profile after injecting 1 PV of water at the location of observation well 2 which is half way between injector and producer (perm 1 and Pc2).
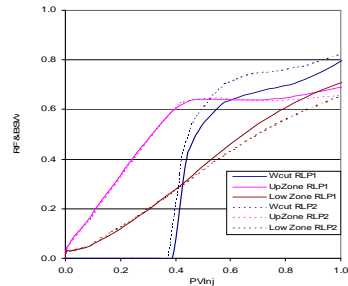
Figure 14: Recovery factor of the upper and lower zones and water cut of two different runs using perm1, Pc1 and RLP1&RLP2.
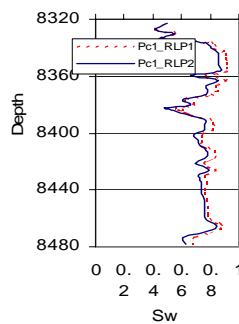
Figure 15: Saturation profile after injecting 1 PV of water at the location of observation well 2, half way between injector and producer (perm 2, Pc1).